Scripta Materialia 138 (2017) 57–61

Contents lists available at ScienceDirect

Scripta Materialia

journal homepage: www.elsevier.com/locate/scriptamat

Regular article

Stability of nanoclusters in an oxide dispersion strengthened alloy under neutron irradiation

Xiang Liu [a], Yinbin Miao [b], Yaqiao Wu [c,d], Stuart A. Maloy [e], James F. Stubbins [a,f,*]

[a] Department of Nuclear, Plasma, and Radiological Engineering, University of Illinois at Urbana-Champaign, Urbana, IL 61801, USA
[b] Nuclear Engineering Division, Argonne National Laboratory, Lemont, IL 60439, USA
[c] Department of Materials Science and Engineering, Boise State University, Boise, ID 83725, USA
[d] Center for Advanced Energy Studies, Idaho Falls, ID 83401, USA
[e] Materials Science and Technology Division, Los Alamos National Laboratory, Los Alamos, NM 87545, USA
[f] International Institute for Carbon Neutral Energy Research (WPI-I2CNER), Kyushu University, 744 Motooka, Nishi-ku, Fukuoka 819-0395, Japan

ARTICLE INFO

Article history:
Received 16 March 2017
Received in revised form 27 April 2017
Accepted 16 May 2017
Available online xxxx

Keywords:
Oxide dispersion strengthened (ODS) alloy
Microstructure
Atom probe tomography
Neutron irradiation

ABSTRACT

Here, we report atom probe tomography results of the nanoclusters in a neutron-irradiated oxide dispersion strengthened alloy. Following irradiation to 5 dpa at target temperatures of 300 °C and 450 °C, fewer large nanoclusters were found and the residual nanoclusters tend to reach an equilibrium Guinier radius of 1.8 nm. With increasing dose, evident decrease in peak oxygen and titanium (but not yttrium) concentrations in the nanoclusters was observed, which was explained by atomic weight, solubility, diffusivity, and chemical bonding arguments. The chemical modifications indicate the equilibrium size is indeed a balance of two competing processes: radiation enhanced diffusion and collisional dissolution.

Oxide dispersion strengthened (ODS) alloys are promising structural materials for advanced reactor systems. By introducing nanoclusters into the metallic matrix using mechanical alloying (MA), ODS alloys show excellent high-temperature mechanical strength and superior irradiation resistance [1]. It is well known that the nanoclusters play important roles in both maintaining the mechanical strength by pinning dislocations and enhancing radiation tolerance by providing extra sinks for irradiation-induced point defects and helium atoms. Therefore, understanding the properties of the nanoclusters and their behavior under extreme conditions such as high temperatures and intense neutron irradiation is important for both fundamental research and the development of resilient materials for advanced nuclear reactors.

This study focuses on a commercial ferritic ODS alloy, MA957, that was developed in the 1980s by the International Nickel Company (INCO) [2]. Previous studies have been carried out to investigate the nanoclusters in unirradiated MA957, especially on their stoichiometry and crystal structures [3,4], chemical composition-size correlation [5], and stability at high temperatures [6,7]. Current findings show that both nonstoichiometric Y-Ti-O nanoclusters and stoichiometric $Y_2Ti_2O_7$ particles exist in MA957. Smaller (2–10 nm diameter) nanoclusters are more likely to be nonstoichiometric with a Y/Ti ratio <1 [5,6], and larger (>15 nm diameter) nanoclusters are more likely to be stoichiometric $Y_2Ti_2O_7$ particles with a cubic pyrochlore structure [5,8].

The stability of the nanoclusters in ODS alloys under irradiation is much more complicated. In principle, the size, structure, and chemical composition of precipitates can be altered by irradiation. Various previous studies have reported that the size of the nanoclusters was reduced after irradiation [9–12], and some also reported concurrent increase in number density [13]. In other studies, the nanoclusters were reported to be stable under irradiation [14,15]. In yet another investigation, the number density of the nanoclusters was reported to be reduced but the size remained about the same after irradiation [16]. The irradiation response of these nanoclusters is not well understood, partially due to the lack of systematic atomic scale experimental data. For MA957, only a few studies have investigated the nanoclusters under neutron irradiation condition: the nanoclusters were reported stable (except for slight decrease in number density) after been neutron-irradiated to 3 dpa at 600 °C [14], 75 dpa at 430 °C [8], and 109–121 dpa at 412 °C–670 °C [17]. Although the nanoclusters in these studies were found to be stable, little chemical information was provided. Therefore, it is not clear whether radiation affects the chemical composition of the nanoclusters or not. It is also not clear whether the formerly observed stability of the nanoclusters holds under different irradiation conditions than those previously examined.

The material used in this study was mechanical-alloyed ODS alloy MA957, with a nominal composition of Fe-13.87Cr-0.014C-1.5Ti-0.3Mo-0.13Ni-0.1Al-0.083Co-0.22Y_2O_3, in wt.%. The specimens were

* Corresponding author at: 216 Talbot Laboratory, 104 South Wright Street, Urbana, IL 61801, USA.
E-mail address: jstubbin@illinois.edu (J.F. Stubbins).

http://dx.doi.org/10.1016/j.scriptamat.2017.05.023
1359-6462/

irradiated in the Advanced Test Reactor (ATR), Idaho National Laboratory. The target irradiation temperatures were 300 °C and 450 °C, and the target doses were 0.1 dpa, 1.0 dpa, and 5.0 dpa. The estimated actual specimen temperatures and doses were obtained from as-run analysis and were listed in Table 1. The sample ID is named as Material Name_Target Dose_Target Temperature. As can be seen from Table 1, the estimated temperatures and doses deviated from the target temperatures and doses. For instance, MA957_5.0_300 specimens were actually irradiated at ~380 °C ± 32 °C to 4.15 dpa. For the same target irradiation temperature, the 0.1 dpa specimens have the lowest irradiation temperature. The irradiations for 1.0 dpa specimens were completed in one cycle. The 5.0 dpa specimens underwent three cycles and therefore have the largest variance in the irradiation temperature. For simplicity, all the irradiation temperatures and doses mentioned in the following discussions refer to the target temperatures and doses.

The post-irradiation examination (PIE) was carried out at the Microscopy and Characterization Suite (MaCS), Center for Advanced Energy Studies (CAES). Atom probe tips were prepared by focused ion beam (FIB) lift-out and annular milling using a FEI Quanta 3D FEG DualBeam FIB/SEM. The atom probe tomography (APT) experiments were performed on a CAMECA LEAP 4000× HR. The APT specimens were analyzed in the 200 kHz pulsed-laser mode at a specimen temperature of 50 K, and a focused laser beam energy of 50 or 70 pJ. Data analysis was performed using the CAMECA IVAS software.

The nanoclusters in both unirradiated and neutron-irradiated MA957 specimens were characterized using the maximum separation method and isoconcentration surfaces (isosurfaces) [14,18,19]. In the maximum separation method, the parameters were chosen as $d_{max} = 0.69$ nm, $n_{min} = 20$, and $L = d_{erosion} = 0.5$ nm. The sizes of the nanoclusters were measured using the Guinier radius r_G, which is related to the radius of gyration r_g by $r_G = \sqrt{5/3} r_g$ [19]. The number densities of the nanoclusters were estimated from the number of nanoclusters divided by the analyzed specimen volume, with a lattice constant of $a = 2.88$ Å. On average, the total number of collected ions for one irradiation condition was around 30 M, representing an analyzed volume of 1×10^6 nm^3.

Fig. 1(a) shows the atom maps and nanocluster distribution in the unirradiated condition. The nanoclusters were obtained using the maximum separation method. The number density of the nanoclusters in the unirradiated sample is around 9.2×10^{22} m^{-3}. It can be clearly seen that all the nanoclusters are enriched in yttrium, titanium, and oxygen. Only the largest two nanoclusters are also enriched in aluminum as shown in the Al map in Fig. 1(a). A close-up of a large (~10 nm) nanocluster is shown in Fig. 1(b). The clustering of Al, O, Ti, and Y can be readily observed. It is also noticed that the Al atoms and O atoms are relatively more loosely distributed, while Ti and Y atoms are more concentrated towards the interior of the nanocluster.

The observed large nanoclusters seems to be a transitional nonstoichiometric Y-Al-Ti-O state between the small (~2 nm) Y-Ti-O nanoclusters commonly observed in ODS FeCr alloys and the larger (tens of nm) Y-Al-O phases (YAG, YAM, YAP, and YAH) found in ODS FeCrAl alloys [20–22], when Al is available in limited amount (~0.1 wt.% for MA957).

The nanoclusters in neutron-irradiated samples were analyzed using the maximum separation method with similar parameters. Fig. 2 shows the size distribution histograms, mean Guinier radii, and number density of the nanoclusters in MA957 at different irradiation conditions. On average around 150 nanoclusters were analyzed for each condition.

The histograms in Fig. 2(a)–(e) clearly show that the size distribution of the nanoclusters became narrower with increasing dose, at both 300 °C and 450 °C. The percentage of large nanoclusters (r_G > 2.5 nm) dropped noticeably in the 5.0 dpa specimens, indicating that some large nanoclusters have been dissolved by displacive collision processes during neutron irradiation. Fig. 2(f) shows the mean Guinier radius of the nanoclusters at different irradiation conditions. The mean Guinier radius tends to converge as the dose increases. At 5.0 dpa, the average Guinier radii of the nanoclusters in the samples irradiated at 300 °C and 450 °C are about 1.78 ± 0.05 nm, and 1.80 ± 0.06 nm, respectively.

The average number densities of the nanoclusters at different irradiation conditions are shown in Fig. 2(g). No apparent trend was found and the number density remained the same order of magnitude (~10^{23} n/m^3) in all analyzed samples. This indicates that under neutron irradiation, although the larger nanoclusters tend to be dissolved, small nanoclusters are more stable. The overall number density of the nanoclusters was not affected since large nanoclusters only account for a very small fraction of the total.

The data in Fig. 2 should be interpreted cautiously, remembering that the distribution of the nanoclusters in ODS alloys can be inhomogeneous. In Fig. 2(f), the average radius at 0.1 dpa_300 °C is higher than that of the unirradiated condition, which should be due to the inherent nonuniformity and limited APT data sampling rather than neutron irradiation. However, the general trend shown by the decrease in the standard deviation with increasing dose in Fig. 2(f) still reveals that in the investigated temperature and dose range, neutron irradiation is likely to dissolve large nanoclusters and the Guinier radii of the smaller nanoclusters tend to approach 1.8 nm. In other words, neutron irradiation tends to homogenize the size distribution of the nanoclusters by dissolving larger nanoclusters.

Displacive collisions and radiation enhanced back-diffusion are two competing processes affecting the stability of precipitates under irradiation [10]. On one hand, under energetic neutron bombardments, atoms are displaced from their original lattice sites by collision cascades. If the atoms of the nanoclusters reside in the collision cascades, the nanoclusters could then be dissolved or at least, partially dissolved. On the other hand, neutron irradiation also produces defects in excess of their equilibrium concentration, resulting in radiation-enhanced diffusion (RED). Displaced nanocluster atoms could diffuse back into the nanoclusters through RED, leading to the recovery or growth of the nanoclusters. Although the displacive collision and back-diffusion cannot be directly detected experimentally, these two processes can be separately inspected through low-temperature irradiation and subsequent annealing. Certain et al. [23] observed significant cluster dissolution in an ODS steel irradiated at −75 °C, and the nanoclusters reassembled after subsequent annealing at 850 °C.

From the aforementioned nanocluster size analysis, it is suggested that the large nanoclusters were more likely to be dissolved, which was apparently due to collisional events induced by energetic neutron bombardments. However, the small nanoclusters tend to reach an equilibrium size of $r_G \cong 1.8$ nm, rather than being dissolved. This indicates that RED helped nanocluster recovery in the investigated irradiation conditions. The larger nanoclusters cannot survive well due to higher dissolution rate compared to the growth rate limited by back diffusion. The RED process has also been affirmed indirectly by the observed radiation-enhanced Cr-rich α′ precipitation and radiation-induced minor element segregation at the nanocluster interfaces in irradiated specimens, which will be reported in another separate study.

In addition to the size and density measurements, proximity histograms (proxigrams) produced from 1.0 at.% Y isosurfaces were used to examine the chemical modifications of the nanoclusters. Two groups of nanoclusters in different sizes were chosen to illustrate the size effect.

Table 1
Target and simulated irradiation conditions of MA957.

Sample ID	$T_{irr.}$ (°C)	dpa
MA957-0.1-300	287 ± 7	0.12
MA957-0.1-450	417 ± 10	0.12
MA957-1.0-300	340 ± 15	1.02
MA957-1.0-450	478 ± 14	0.68
MA957-5.0-300	380 ± 32	4.15
MA957-5.0-450	498 ± 36	3.9

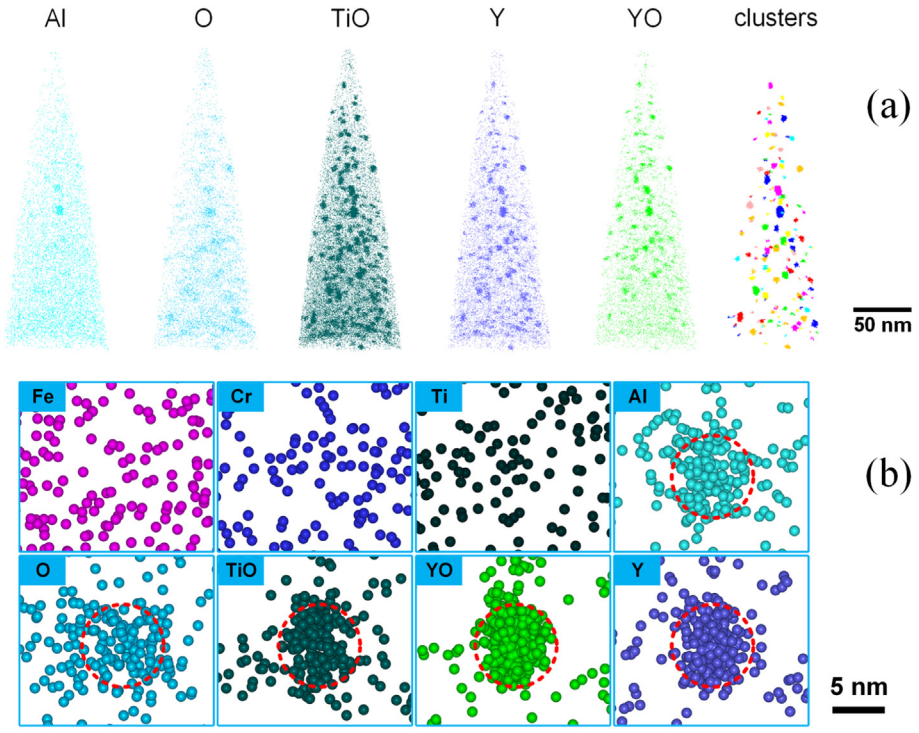

Fig. 1. (a) Atom maps and reconstructed nanocluster distribution in unirradiated MA957, (b) enlarged view of the atom maps showing the clustering of Al, O, Ti, and Y in a large nanocluster.

Fig. 3 shows the proxigrams of the nanoclusters in the unirradiated condition. It is easy to see that the elemental composition of the nanoclusters was highly size-dependent: larger nanoclusters (r > 3 nm) in Fig. 3(a) have much higher peak Y, Ti, O concentrations and higher Y/Ti ratio. Similar size dependence in ODS alloys has been reported in previous studies [3,5,24].

In order to avoid the uncertainties due to the size effect, only nanoclusters in the range of 1.5 nm to 2.0 nm were chosen in the following peak concentration analysis, and on average 50–80 clusters were included for each condition. The peak Y, Ti, and O concentrations of different irradiation conditions were compared to investigate the chemical modifications.

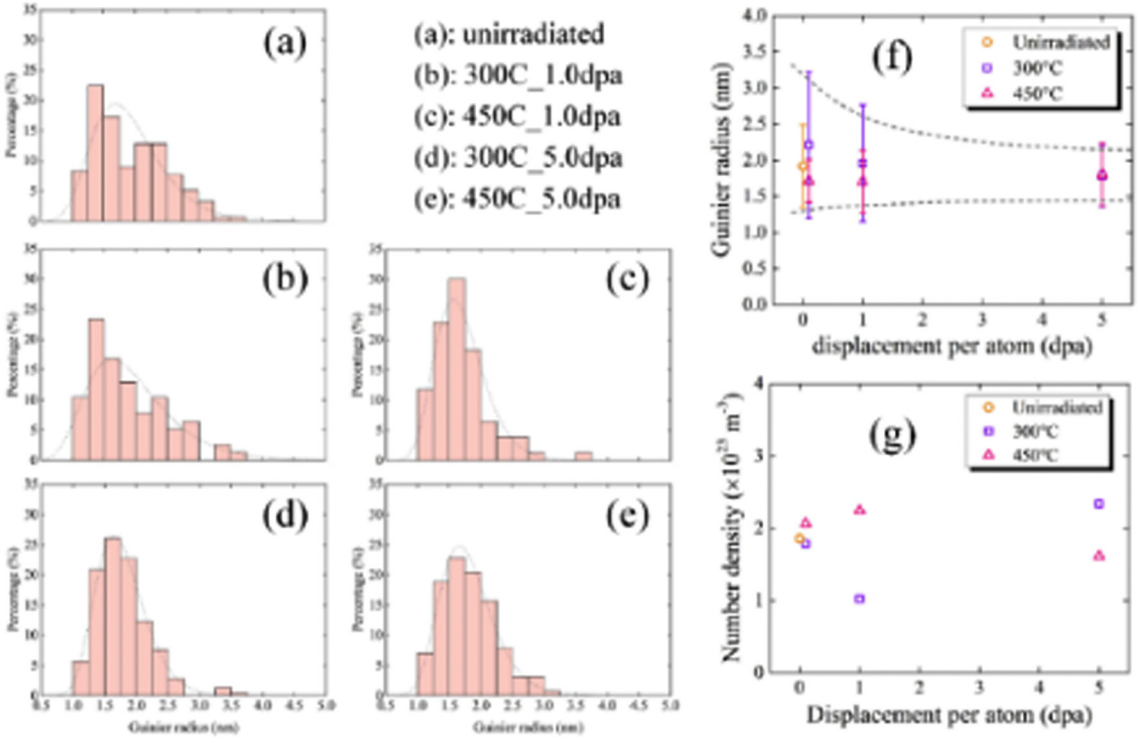

Fig. 2. (a) to (e): Size distribution histograms of the nanoclusters in unirradiated and irradiated conditions; (f): Mean Guinier radii of the nanoclusters at different dose and temperature conditions (dashed curves are for visual aide only); (g): Number density of the nanoclusters at different dose and temperature conditions.

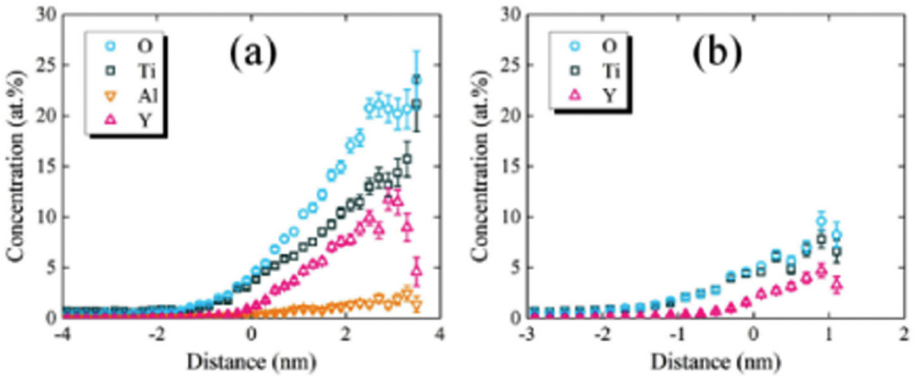

Fig. 3. The proxigrams of selected nanoclusters in unirradiated MA957: (a) radius larger than 3.0 nm, and (b) radius between 1.5 nm and 2.0 nm.

Fig. 4(a) and (b) show the peak Y, Ti, and O concentrations of the nanoclusters in MA957 irradiated to different doses at 300 °C and 450 °C, respectively. At both temperatures, the peak concentrations of O and Ti reduced with increasing dose. The reduction occurred as early as 0.1 dpa. The difference is that the variation at 300 °C was more pronounced than that at 450 °C: the peak concentration of Ti in the unirradiated samples was 7.83 at.%, which reduced to 4.47 at.% at 300 °C, and 6.91 at.% at 450 °C; the peak concentration of O reduced from 9.58 at.% to 5.03 at.% at 300 °C, and 6.77 at.% at 450 °C. The less apparent reduction at higher temperature should be due to increased RED against displacive collisions.

Fig. 4 also shows that the reduction of O peak concentration with increasing dose was most apparent, and the reduction of Y peak concentration was almost unnoticeable. This should be related to the atomic weight, solubility limit, diffusivity, and chemical bonding of O, Ti, and Y atoms.

The relative atomic weight of atom of a particular type of atoms decides its relative stability against displacive collisions. Neutron bombardment displaces O ($A = 16$) and Ti ($A = 48$) atoms much more efficiently than Y ($A = 89$) atoms. For the same incident neutron energy, the average energy transferred to an O atom is about 2.8 times the energy transferred to a Ti atom and 5 times the energy transferred to a Y atom. Therefore, the displacive collisions will knock much more O atoms than Y atoms out of the nanoclusters, and the number of knocked-out Ti atoms lies in between.

The solubility sets the limit of how many knocked-out atoms will diffuse back to the original nanocluster or form new nanoclusters, if the diffusivity of the atoms is high enough. The chemical bonding determines the types of nanoclusters that will form.

O atoms are chemically unstable and in addition to Y-Ti-O nanoclusters, O can form other oxide clusters such as Cr-O and Fe-O clusters, and these clustered O atoms cannot diffuse back to the Y-Ti-O clusters. Also considering that the number of knocked-out O atoms is the highest, the most apparent reduction in O peak concentration is thus expected.

Unlike the various reaction paths of O, knocked-out Ti atoms are more likely to diffuse back into the Y-Ti-O nanoclusters, as indicated by the fact that during the fabrication of ODS steels, Y-Ti-O clusters replaced the original Y_2O_3 particles after hot extrusion or hot isostatic pressing. The less apparent decrease in Ti peak concentration can be explained by fewer knock-out events and reaction paths.

Y has a very low solubility in α-iron (~0.01 at.% at 450 °C) [10,25], and it is almost exclusively found in Y-Ti-O clusters. Therefore, through RED, most of the knocked-out Y atoms will diffuse back to the original Y-Ti-O cluster. The fewest knock-out events, low solubility, and strong bonding with O and Ti atoms, leads to the insignificant variation in the Y peak concentration under irradiation.

In summary, the APT results show that in the investigated temperature (300 °C and 450 °C) and dose regime (up to 5 dpa), the nanoclusters in neutron-irradiated MA957 tend to reach an equilibrium Guinier radius of 1.8 nm, and large nanoclusters are more likely to undergo shrinkage or dissolution. Peak O, Ti, and Y concentrations of the small nanoclusters (1.5 nm to 2.0 nm) were obtained from proxigrams. The levels of O and Ti in the nanoclusters show an apparent reduction after neutron irradiation. The magnitude of reduction was found to be larger at lower temperature, when less diffusional recovery is expected. The chemical analyses indicate although the small nanoclusters did not shrink or dissolve under neutron irradiation, displacive collision and diffusional recovery results in a redistribution of the atoms inside the nanoclusters. It is also inferred that the atomic weight of a particular type of atoms influences its relative stability against displacive collisions, the solubility and chemical bonding determines the stability through radiation-enhanced back diffusion.

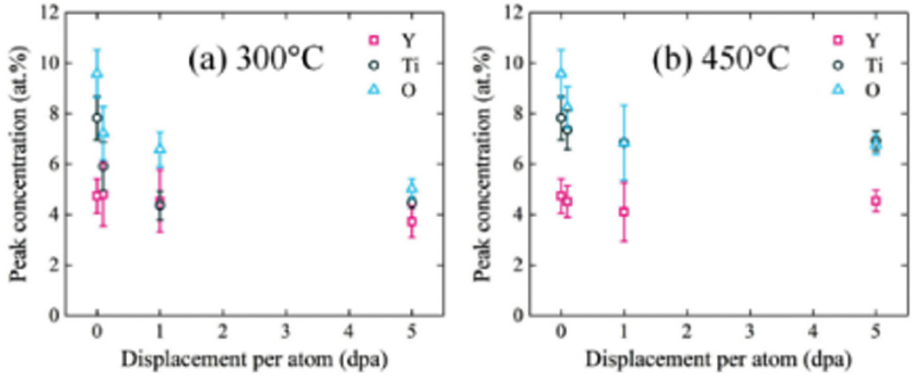

Fig. 4. The peak Y, Ti, and O concentrations of the nanoclusters at different doses irradiated at (a) 300 °C, and (b) 450 °C.

Acknowledgement

This work was funded by Department of Energy's NEUP program DOE INL 00127139. The RTE projects 15-538 and 15-539 were supported by the U.S. Department of Energy, Office of Nuclear Energy under DOE Idaho Operations Office Contract DE-AC07-051D14517 as part of a Nuclear Science User Facilities experiment. The authors would like to thank Jatuporn Burns and Allyssa Bateman at the Center for Advanced Energy Studies for assisting with the FIB sample preparation. They would also like to thank NSUF staff Collin Knight and MaCS Lab lead Joanna Taylor for their help with coordinating the projects.

References

[1] G.R. Odette, M.J. Alinger, B.D. Wirth, Annu. Rev. Mater. Res. 38 (2008) 471–503.
[2] J.J. Fischer, Dispersion Strengthened Ferritic Alloy for Use in Liquid Metal Fast Breeder Reactors, 1978.
[3] A. Hirata, T. Fujita, Y.R. Wen, J.H. Schneibel, C.T. Liu, M.W. Chen, Nat. Mater. 10 (2011) 922–926.
[4] Y. Wu, E.M. Haney, N.J. Cunningham, G.R. Odette, Acta Mater. 60 (2012) 3456–3468.
[5] H. Sakasegawa, L. Chaffron, F. Legendre, L. Boulanger, T. Cozzika, M. Brocq, Y. de Carlan, J. Nucl. Mater. 384 (2009) 115–118.
[6] H. Sakasegawa, F. Legendre, L. Boulanger, M. Brocq, L. Chaffron, T. Cozzika, J. Malaplate, J. Henry, Y. De Carlan, J. Nucl. Mater. 417 (2011) 229–232.
[7] M.K. Miller, D.T. Hoelzer, E.A. Kenik, K.F. Russell, Intermetallics 13 (2005) 387–392.
[8] J. Ribis, S. Lozano-Perez, J. Nucl. Mater. 444 (2014) 314–322.
[9] T. Chen, E. Aydogan, J.G. Gigax, D. Chen, J. Wang, X. Wang, S. Ukai, F.A. Garner, L. Shao, J. Nucl. Mater. 467 (2015) 42–49.
[10] T. Chen, J.G. Gigax, L. Price, D. Chen, S. Ukai, E. Aydogan, S.A. Maloy, F.A. Garner, L. Shao, Acta Mater. 116 (2016) 29–42.
[11] T.R. Allen, J. Gan, J.I. Cole, S. Ukai, Nucl. Sci. Eng. 151 (2005) 305–312.
[12] F. Li, H. Abe, T. Ishizaki, Y. Li, T. Nagasaka, T. Muroga, T. Nagase, H. Yasuda, J. Nucl. Mater. 455 (2014) 724–727.
[13] E. Aydogan, N. Almirall, G.R. Odette, S.A. Maloy, O. Anderoglu, L. Shao, J.G. Gigax, L. Price, D. Chen, T. Chen, F.A. Garner, Y. Wu, P. Wells, J.J. Lewandowski, D.T. Hoelzer, J. Nucl. Mater. 486 (2017) 86–95.
[14] M.K. Miller, D.T. Hoelzer, J. Nucl. Mater. 418 (2011) 307–310.
[15] H. Kishimoto, K. Yutani, R. Kasada, O. Hashitomi, A. Kimura, J. Nucl. Mater. 367–370 (2007) 179–184.
[16] S. Yamashita, N. Akasaka, S. Ukai, S. Ohnuki, J. Nucl. Mater. 367–370 (2007) 202–207.
[17] N.A. Bailey, E. Stergar, M. Toloczko, P. Hosemann, J. Nucl. Mater. 459 (2015) 225–234.
[18] D. Vaumousse, A. Cerezo, P.J. Warren, Ultramicroscopy 95 (2003) 215–221.
[19] C.A. Williams, E.A. Marquis, A. Cerezo, G.D.W. Smith, J. Nucl. Mater. 400 (2010) 37–45.
[20] K.A. Unocic, B.A. Pint, D.T. Hoelzer, J. Mater. Sci. 51 (2016) 9190–9206.
[21] C.H. Zhang, A. Kimura, R. Kasada, J. Jang, H. Kishimoto, Y.T. Yang, J. Nucl. Mater. 417 (2011) 221–224.
[22] G. Zhang, Z. Zhou, K. Mo, P. Wang, Y. Miao, S. Li, M. Wang, X. Liu, M. Gong, J. Almer, J.F. Stubbins, J. Alloys Compd. 648 (2015) 223–228.
[23] A. Certain, S. Kuchibhatla, V. Shutthanandan, D.T. Hoelzer, T.R. Allen, J. Nucl. Mater. 434 (2013) 311–321.
[24] Y. Miao, K. Mo, Z. Zhou, X. Liu, K.-C. Lan, G. Zhang, M.K. Miller, K.A. Powers, J.F. Stubbins, J. Nucl. Mater. 480 (2016) 195–201.
[25] H. Okamoto, J. Phase Equilib. 16 (1995) 1995.